Advances in Military Technology
Vol. 19, No. 1, 2024, pp. 71-98
ISSN 1802-2308, eISSN 2533-4123
DOI 10.3849/aimt.01858

An Airframe Stabilization System with State Observer and Correction Part for Terminal-Phase Missile Guidance

W. Bużantowicz*

Faculty of Mechatronics, Armament and Aerospace, Military University of Technology, Warsaw, Poland

The manuscript was received on 25 September 2023 and was accepted after revision for publication as research paper on 31 March 2024.

Abstract:

In this paper an airframe stabilization system with state observer and correction part for a canard-controlled anti-aircraft missile is presented. The state observer based system is designed to be easy to implement and undemanding of significant onboard data processing and CPU resources. In addition, the correction part to improve the system's capabilities is described and an analytical method for determining its settings is proposed. The paper considers the terminal phase of guiding an anti-aircraft missile against an aerial target. This is of particular interest when considering the issues of combating the current means of air attack, characterized by high maneuverability, effectively. Robustness to disturbances in the signal processing paths and the ability to effectively stabilize the airframe is presented with extensive simulations of the proposed system using the Monte Carlo method.

Keywords:

stabilization system, autopilot, state observer, terminal-phase guidance

1 Introduction

The dynamic development of missile technology observed in recent decades has resulted in a range of advances, such as improved algorithms for controlling and stabilizing missile flight. This is particularly important in the case of anti-aircraft missiles, where their range of tasks has been significantly expanded in response to the dynamic development of modern air strike means, their combat capabilities, and tactics of use.

Ensuring the stabilization of the anti-aircraft missile airframe is usually necessary during every phase of its flight. In the launch phase, stabilization is required due to the

* *Corresponding author: Faculty of Mechatronics, Armament and Aerospace, Military University of Technology, Gen. S. Kaliskiego 2 Street, PL 00-908 Warsaw, Poland. E-mail: witold.buzantowicz@wat.edu.pl. ORCID 0000-0002-4737-4857*

rapid increase in the missile velocity, as well as the instability of the system characteristics, resulting from changes in environmental parameters as the missile altitude increases, as well as changes to the geometry and mass of the missile itself (e.g. resulting from the consumption of fuel or dropping rocket booster). During midcourse, the stabilization system plays an important role in determining the missile flight trajectory, and in particular it enables the reduction of energy losses as the airframe travels through the atmosphere. The stabilization system role is, however, most evident in the terminal guidance phase (a distance of several kilometers), when the missile switches to self-guidance mode based on indications of the onboard seeker. Movement of the airframe has been observed to adversely affect the operation of the coordinate determination system [1, 2]. Every change in direction of the missile flight velocity vector caused by the deflection of the fins, which changes the angle of attack and forces the airframe to rotate with the aerodynamic control torque, causes transient processes that negatively affect the operating conditions of the seeker installed in the nose section [3]. It is important to consider that the high maneuverability of modern air attack assets enables them to react to threats, e.g. by performing missile evasion maneuvers. This poses particular problems during the terminal phase of target tracking, as it forces the missile to react quickly, introducing significant dynamic errors into the system, disrupting the operating conditions of the seeker, and increasing the error rate of motion coordinates in the guidance signals. This results in increased tracking errors, and in extreme cases, the target tracking process may even break.

The first attempts to use stabilization systems in anti-aircraft missiles date back to the 1940s. Late in World War II, the German C-2 Wasserfall missiles were equipped with simple systems that used three-axis angular rate gyroscopes [4]. The three-loop autopilot (TLA) system, developed by Raytheon in the 1960s, proved to be a milestone in the development of stabilization systems [5, 6], and is still widely used and referenced in scientific discussion, see e.g. [7-10].

Nowadays, there are two main approaches to the problem of stabilizing the static and dynamic characteristics of anti-aircraft missile airframes. In the classical one, an architecture separates guidance and flight control functions [5, 11-15], and several assumptions are made to simplify the system dynamics. It is necessary to note the potential dangers of this approach, especially from a robustness point of view. After linearization, the control action can be very sensitive to omitted high-order terms, i.e. not stable in Lyapunov sense [3]. However, the linear time-invariant (LTI) model assumption is valid for a finite, short-time horizon about a given operating point and can be efficiently used to analyze the problems connected with the terminal phase of missile guidance [16, 17]. Modern research focuses on satisfying performance and stability robustness requirements by designing missile autopilots as a component part of a common guidance and control loop. This approach is generally known as integrated guidance and control (IGC) [12, 13, 18, 19]. IGC design methods take advantage of the coupling relationship between guidance and control system; they can significantly enhance missile performance in comparison with the classical system architecture [20], as well as information on the missile-target relative motion, attitude angle, and airframe overload.

In this context, the use of observers constitutes an important part of the research work on the area in question [21]. In recent years, many different observer-based control schemes have been proposed to stabilize missile airframe characteristics, including e.g. linear and enhanced extended state and disturbance observers [22, 23, 24], reduced order

observers [25], H_∞ observers [26], sliding mode control techniques [27, 28, 29], and more others.

The aim of this paper is to present an airframe stabilization system with a dedicated state observer and correction part for a canard-controlled anti-aircraft missile. Issues related to the effectiveness of the proposed solutions in the absence and presence of disturbances in the signal processing paths are discussed. The paper considers the terminal phase of homing an anti-aircraft missile onto an aerial target. This phase is of particular interest due to issues related to the effectiveness of counteracting means of air attack currently in use, characterized by their high maneuverability. Contemporary combat considerations mean that the accuracy of tracking aerial targets by anti-aircraft missiles is of key importance for completing the assigned combat task, i.e. eliminating the threat and ensuring the survival of the defended objects.

The main contributions of the article can be summarized as follows:

- the missile airframe dynamics is modeled in the form of a matrix representation for the ease of designing the controller;
- state observer (SO) based missile stabilization system is designed as easy to implement and undemanding of significant onboard data processing and CPU resources;
- the state observer's correction part (SO+CP) to improve system capabilities is described and an analytical method for determining its settings is proposed;
- robustness to disturbances in the signal processing paths and the ability to effectively stabilize the airframe is presented through extensive simulations using the Monte Carlo method and in relation to a classical three-loop autopilot (TLA) structure.

The paper is composed as follows. In Section 2, the missile airframe dynamics model used in the stabilization system design is discussed and the state observer based stabilization systems with and without correction part are described. To show the validity of the proposed controllers, numerical simulations have been performed and their results are given in Section 3. Finally, conclusions of this study are offered in Section 4.

2 Methods

In this section, a state-observer based missile stabilization system with correction part is described. First, the missile airframe dynamics model is derived in vector-matrix form. Next, the state observer based autopilot (SO) is presented and a selection of coefficients of its gain matrix $\boldsymbol{K}$ is commented on. The issues related to system stability and compensation of its gain non-stationarity are discussed, and a stabilization system with correction part (SO+CP) is finally proposed.

2.1 Missile Dynamics Model

In terms of control, the motion of a canard-controlled missile (Fig. 1) can be described using the following system of differential equations:

$$\dot{\alpha} = -\frac{T}{mV}\sin\alpha - \frac{\rho V}{2m}Sc_L(Ma,\alpha) + \omega - \frac{\rho V}{2m}Sc_C(Ma,\alpha,\delta) \tag{1}$$

$$\dot{\omega} = -\frac{\rho V^2}{2I} Slc_M^{\alpha}(Ma,\alpha) - \frac{\rho V}{2I} Sl^2 c_M^{\omega}(Ma,\omega) + \frac{\rho V^2}{2I} Slc_M^{\delta}(Ma,\alpha,\delta) \tag{2}$$

The symbols used in Eqs (1)-(2) mean as follows: T is the thrust [N]; m is the missile mass [kg]; I is the airframe moment of inertia [kg·m^2]; V is the module of missile velocity vector [m/s]; Ma is Mach's number [–]; ω is the airframe angular rate [rad/s]; α is the angle of attack [rad]; δ is the canard fin deflection angle [rad]; ρ is the air density [kg/m^3]; S is the reference area [m^2]; l is the reference length [m]; c_L and c_C are lift force related aerodynamic coefficients of the missile airframe and canards [–], respectively; c_M^{ω} is the damping coefficient [–]; c_M^{α} and c_M^{δ} are aerodynamic moment coefficients related to missile airframe and canards [–], respectively. Assuming that gravity force acting on the airframe is treated as an external excitation compensated by a component added to the control signal, Eqs (1)-(2) can be used to describe the missile dynamics both in the yaw and pitch control planes.

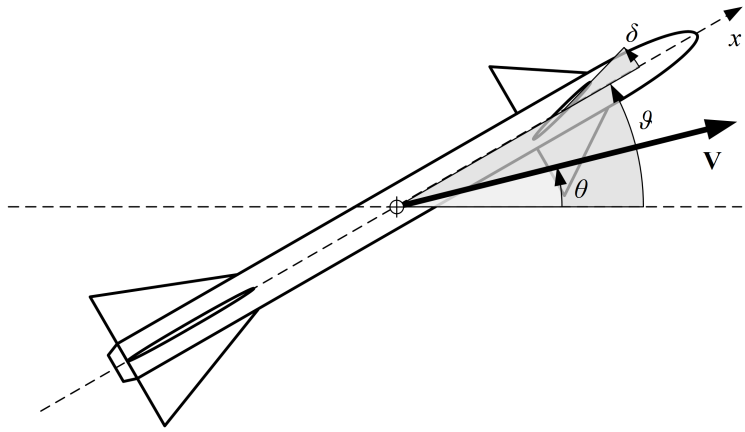

Fig. 1 Canard-controlled missile configuration

For the purposes of designing the stabilization system, assuming that the coefficients of aerodynamic forces and moments are linearly dependent on the variables α, ω and δ, and linearizing the sine function for small values of the angle of attack, a linearized system of equations describing the missile dynamics in the control plane is obtained:

$$\dot{\alpha} = -\left\{ \frac{\rho V}{2m} S[c_L(Ma) + c_C(Ma)] + \frac{T}{mV} \right\} \alpha + \omega - \frac{\rho V}{2m} Sc_C(Ma)\delta \tag{3}$$

$$\dot{\omega} = -\left\{ \frac{\rho V^2}{2I} Sl \left[c_M^{\alpha}(Ma) - c_M^{\delta}(Ma) \right] \right\} \alpha - \frac{\rho V}{2I} Sl^2 c_M^{\omega}(Ma)\omega + \frac{\rho V^2}{2I} Slc_M^{\delta}(Ma)\delta \tag{4}$$

After introducing the following coefficients for notational reasons:

$$a_1 = \frac{\rho V}{2m} S\left[c_L(Ma) + c_C(Ma)\right] + \frac{T}{mV} \qquad a_2 = \frac{\rho V^2}{2I} Sl\left[c_M^{\alpha}(Ma) - c_M^{\delta}(Ma)\right]$$

$$a_3 = \frac{\rho V}{2I} Sl^2 c_M^{\omega}(Ma) \tag{5}$$

$$b_1 = \frac{\rho V}{2m} S c_C(Ma) \qquad b_2 = \frac{\rho V^2}{2I} Sl c_M^{\delta}(Ma)$$

and switching to vector-matrix notation, an equivalent form of the system described by Eqs (3)-(4) is obtained:

$$\begin{bmatrix} \dot{\alpha} \\ \dot{\omega} \end{bmatrix} = \begin{bmatrix} -a_1 & 1 \\ -a_2 & -a_3 \end{bmatrix} \begin{bmatrix} \alpha \\ \omega \end{bmatrix} + \begin{bmatrix} -b_1 \\ b_2 \end{bmatrix} \delta \tag{6}$$

$$\omega = \begin{bmatrix} 0 & 1 \end{bmatrix} \begin{bmatrix} \alpha \\ \omega \end{bmatrix} \tag{7}$$

or concisely

$$\begin{cases} \dot{\boldsymbol{x}} = \boldsymbol{A}\boldsymbol{x} + \boldsymbol{B}\delta \\ \boldsymbol{y} = \boldsymbol{C}\boldsymbol{x} \end{cases} \tag{8}$$

where

$$\boldsymbol{x} = \begin{bmatrix} \alpha \\ \omega \end{bmatrix} \qquad \boldsymbol{y} = \omega \qquad \boldsymbol{A} = \begin{bmatrix} -a_1 & 1 \\ -a_2 & -a_3 \end{bmatrix} \qquad \boldsymbol{B} = \begin{bmatrix} -b_1 \\ b_2 \end{bmatrix} \qquad \boldsymbol{C} = \begin{bmatrix} 0 & 1 \end{bmatrix} \tag{9}$$

Eq. (8) is supplemented by the following relations:

$$\vartheta = \int \omega \, \mathrm{d}t \qquad a = V\dot{\theta} \qquad \alpha \equiv \vartheta - \theta \tag{10}$$

where: ϑ is the airframe angle [rad], and a is the normal acceleration in the control plane [m/s^2], and by the equation describing the operation of the canard fin servos:

$$\dot{\delta} = \frac{1}{\tau}\left(\delta_{\mathrm{com}} - \delta\right) \qquad \text{and} \qquad |\delta| \le \delta_{\max} \tag{11}$$

where δ, δ_{com} and $\delta_{\max}$ respectively denote: the current, commanded and maximum canard fin deflection angle [rad], while τ is the time constant of the servos [s].

2.2 Stabilization System Design

The state observer proposed for the airframe given by Eqs (8)-(9) is described as follows:

$$\dot{\boldsymbol{z}} = \boldsymbol{A}\boldsymbol{z} + \boldsymbol{B}\kappa + \boldsymbol{L}(v - y) \tag{12}$$

$$v = \boldsymbol{C}\boldsymbol{z} \tag{13}$$

where $\boldsymbol{z}$ is the observer's state vector, v is the observer's output signal, κ is the control signal, and $\boldsymbol{L}$ is the convergence error gain matrix. The state vector recovery error

$$\boldsymbol{e} = \boldsymbol{z} - \boldsymbol{x} \tag{14}$$

assuming for controller design purposes that $\kappa = \delta_{\text{com}} = \delta$ (i.e., the inertia of the canards is ignored), satisfies the equation

$$\dot{\boldsymbol{e}} = (\boldsymbol{A} + \boldsymbol{LC})\,\boldsymbol{e} \tag{15}$$

and the condition for its decay is for the eigenvalues of the matrix $(\boldsymbol{A} + \boldsymbol{LC})$ to be located in the left half-plane of the complex variable s. For the observer to be able to effectively perform the stabilization task, the coefficients of the coupling matrix $\boldsymbol{L}$ of the system and its observer must be selected in such a way that this condition is true for any time t.

The Kalman matrix for Eq. (8) takes the following form:

$$\boldsymbol{Q} = \begin{bmatrix} \boldsymbol{C} \\ \boldsymbol{CA} \end{bmatrix} = \begin{bmatrix} 0 & 1 \\ -a_2 & -a_3 \end{bmatrix} \tag{16}$$

Its determinant is different from zero, and its order is equal to 2, which means that the system under consideration is observable. Thus, its observable canonical form (OCF) can be determined by a linear transformation of the state vector

$$\tilde{\boldsymbol{x}} = \boldsymbol{M}\boldsymbol{x} \tag{17}$$

$\boldsymbol{M}$ is a non-singular matrix given as:

$$\boldsymbol{M} = \begin{bmatrix} \zeta_1 \boldsymbol{C} + \boldsymbol{CA} \\ \boldsymbol{C} \end{bmatrix} = \begin{bmatrix} -a_2 & a_1 \\ 0 & 1 \end{bmatrix} \tag{18}$$

where ζ_1 is one of the coefficients of the characteristic polynomial of matrix $\boldsymbol{A}$:

$$\det(s\boldsymbol{I} - \boldsymbol{A}) = s^2 + \zeta_1 s + \zeta_0 = s^2 + (a_1 + a_3)s + a_1 a_3 + a_2 \tag{19}$$

In Eq. (19) $\boldsymbol{I}$ is an identity matrix. Substituting (17) into (8) gives the following equation:

$$\dot{\tilde{\boldsymbol{x}}} = \boldsymbol{MAM}^{-1}\tilde{\boldsymbol{x}} + \boldsymbol{MB}\delta = \tilde{\boldsymbol{A}}\tilde{\boldsymbol{x}} + \tilde{\boldsymbol{B}}\delta \tag{20}$$

in which

$$\tilde{\boldsymbol{A}} = \begin{bmatrix} 0 & -a_1 a_3 - a_2 \\ 1 & -a_1 - a_3 \end{bmatrix} \qquad \text{and} \qquad \tilde{\boldsymbol{B}} = \begin{bmatrix} a_1 b_2 + a_2 b_1 \\ b_2 \end{bmatrix} \tag{21}$$

while the output in Eq. (8) for its OCF is given as follows:

$$y = \tilde{\boldsymbol{C}}\tilde{\boldsymbol{x}} = \boldsymbol{CM}^{-1}\tilde{\boldsymbol{x}} = \boldsymbol{C}\tilde{\boldsymbol{x}} \tag{22}$$

Assuming the observer's characteristic polynomial as

$$\det\left(s\boldsymbol{I} - \tilde{\boldsymbol{A}}\right) = (s + \varsigma)^2 = s^2 + 2\varsigma s + \varsigma^2 = s^2 + \tilde{\zeta}_1 s + \tilde{\zeta}_0 \tag{23}$$

where $\varsigma > 0$, it is required that the reproduction error decay process is non-oscillatory, with a decay rate of at least $ce^{-\varsigma t}$, $c = \text{const}$. The observer's coupling matrix $\tilde{\boldsymbol{L}}$ of the system transformed to the OCF takes the following form:

$$\tilde{\boldsymbol{L}} = \begin{bmatrix} \zeta_0 - \tilde{\zeta}_0 \\ \zeta_1 - \tilde{\zeta}_1 \end{bmatrix} = \begin{bmatrix} a_1 a_3 + a_2 - \varsigma^2 \\ a_1 + a_3 - 2\varsigma \end{bmatrix} \tag{24}$$

whereas the convergence error gain matrix $\boldsymbol{L}$ is equal to

$$\boldsymbol{L} = \boldsymbol{M}^{-1}\tilde{\boldsymbol{L}} = \begin{bmatrix} \frac{1}{a_2}\left(a_1^2 - 2a_1\varsigma + \varsigma^2 - a_2\right) \\ a_1 + a_3 - 2\varsigma \end{bmatrix} \tag{25}$$

It is easy to show that the eigenvalues of the matrix $(\boldsymbol{A} + \boldsymbol{LC})$ are located in the left half-plane of the complex variable s, and therefore the condition of the decaying error of the state vector $\boldsymbol{e}$ is satisfied. The following state observer was therefore defined for the missile airframe described by the Eq. (8):

$$\dot{\boldsymbol{z}} = \begin{bmatrix} -a_1 & 1 \\ -a_2 & -a_3 \end{bmatrix}\boldsymbol{z} + \begin{bmatrix} -b_1 \\ b_2 \end{bmatrix}\kappa + \begin{bmatrix} \frac{1}{a_2}\left(a_1^2 - 2a_1\varsigma + \varsigma^2 - a_2\right) \\ a_1 + a_3 - 2\varsigma \end{bmatrix}(v - y) \tag{26}$$

which ensures the reproduction of the state vector $\boldsymbol{x}$ through the observer's state vector $\boldsymbol{z}$.

In the stabilization system with a state observer described by Eq. (26), an assumption is made that

$$\delta = \boldsymbol{K}\boldsymbol{z} \tag{27}$$

where $\boldsymbol{K}$ is the feedback matrix from the reproduced state vector $\boldsymbol{z}$. Eq. (8) thus takes the following form:

$$\dot{\boldsymbol{x}} = \boldsymbol{A}\boldsymbol{x} + \boldsymbol{BK}\boldsymbol{z} \tag{28}$$

whereas the state observer equation, based on (8), (13) and (26), is rewritten as follows:

$$\dot{\boldsymbol{z}} = \boldsymbol{A}\boldsymbol{z} + \boldsymbol{B}\kappa + \boldsymbol{L}(v - y) = \boldsymbol{A}\boldsymbol{z} + \boldsymbol{B}\kappa + \boldsymbol{LC}(\boldsymbol{z} - \boldsymbol{x}) \tag{29}$$

Based on Eq. (14) and ignoring the inertia of the canard fin servos, i.e. assuming that $\kappa = \delta_{\text{com}} = \delta$, the following Eqs are obtained:

$$\begin{aligned} \dot{\boldsymbol{x}} &= \boldsymbol{A}\boldsymbol{x} + \boldsymbol{BK}(\boldsymbol{e} + \boldsymbol{x}) = (\boldsymbol{A} + \boldsymbol{BK})\boldsymbol{x} + \boldsymbol{BK}\boldsymbol{e} \\ \dot{\boldsymbol{e}} &= \dot{\boldsymbol{z}} - \dot{\boldsymbol{x}} = \boldsymbol{A}\boldsymbol{z} + \boldsymbol{B}\kappa + \boldsymbol{LC}(\boldsymbol{z} - \boldsymbol{x}) - \boldsymbol{A}\boldsymbol{x} - \boldsymbol{B}\delta = (\boldsymbol{A} + \boldsymbol{LC})\boldsymbol{e} \end{aligned} \tag{30}$$

i.e.

$$\begin{bmatrix} \dot{\boldsymbol{x}} \\ \dot{\boldsymbol{e}} \end{bmatrix} = \begin{bmatrix} \boldsymbol{A}\boldsymbol{x} + \boldsymbol{BK} & \boldsymbol{BK} \\ 0 & \boldsymbol{A} + \boldsymbol{LC} \end{bmatrix} \begin{bmatrix} \boldsymbol{x} \\ \boldsymbol{e} \end{bmatrix} \tag{31}$$

Based on Eq. (31), the characteristic equation of the stabilization system with an observer is as follows:

$$\det\left[s\boldsymbol{I} - (\boldsymbol{A} + \boldsymbol{BK})\right]\det\left[s\boldsymbol{I} - (\boldsymbol{A} + \boldsymbol{LC})\right] = 0 \tag{32}$$

which means that an appropriate selection of coefficients of the matrix $\boldsymbol{K}$ enables the acquisition of the desired position of all the roots of the polynomial (32) in the left half-plane of the complex variable s. This enables both the stabilization of the airframe and the disappearance of the error of its state vector reconstruction.

2.3 Selection of Gain Matrix Coefficients

Since

$$\det[s\boldsymbol{I}-(\boldsymbol{A}+\boldsymbol{LC})]=(s+\varsigma)^2 \tag{33}$$

assuming that

$$\boldsymbol{K}=\begin{bmatrix}k_1 & k_2\end{bmatrix} \tag{34}$$

Equation (32) is expanded as follows:

$$(s+\varsigma)^2\left(s^2+\zeta_1 s+\zeta_0\right)=0 \tag{35}$$

where

$$\begin{aligned}\zeta_1&=a_1+a_3+b_1k_1-b_2k_2\\ \zeta_0&=a_1a_3+a_2+k_1(a_3b_1-b_2)-k_2(a_1b_2+a_2b_1)\end{aligned} \tag{36}$$

To ensure that all roots of the polynomial (32) are located in the left half-plane, k_1 and k_2 should be selected so as to satisfy the following system of inequalities:

$$a_1+a_3+b_1k_1-b_2k_2>0 \tag{37}$$

$$a_1a_3+a_2+k_1(a_3b_1-b_2)-k_2(a_1b_2+a_2b_1)>0 \tag{38}$$

The solution of inequality (37) is:

$$k_2<\frac{b_1}{b_2}k_1+\frac{a_1+a_3}{b_2} \tag{39}$$

and the solution of inequality (38) is given as:

$$k_2<\frac{a_3b_1-b_2}{a_1b_2+a_2b_1}k_1+\frac{a_1a_3+a_2}{a_1b_2+a_2b_1} \tag{40}$$

The coefficients of the gain matrix $\boldsymbol{K}$ can be indicated by selecting a point belonging to the common area Ψ of the half-planes bounded by lines described by the following Eqs:

$$k_2=\frac{b_1}{b_2}k_1+\frac{a_1+a_3}{b_2} \tag{41}$$

$$k_2=\frac{a_3b_1-b_2}{a_1b_2+a_2b_1}k_1+\frac{a_1a_3+a_2}{a_1b_2+a_2b_1} \tag{42}$$

However, this choice cannot be arbitrary. Let us consider the problem for example of the values of the missile airframe coefficients: a_1 = 5 s^{-1}, a_2 = 2 350 s^{-2}, a_3 = 10 s^{-1}, b_1 = 0.4 s^{-1}, b_2 = 420 s^{-2}. Selecting a random point belonging to area Ψ (Fig. 2a) does not ensure the correct operation of the stabilization system (Fig. 2b). However, based on the obtained results, we can state that the setting values should be sought at the edges of the Ψ area.

Given the above, the following method of selecting the $\boldsymbol{K}$ matrix coefficients is proposed. Starting from the point of line intersection described by Eqs (41)-(42)

$$\begin{aligned}K_0&=\left(\frac{\gamma_{num}}{\gamma_{den}},\frac{b_1\gamma_{num}+\gamma_{den}(a_1+a_3)}{b_2\gamma_{den}}\right)\\ \gamma_{num}&=-(a_1+a_3)(a_1b_2+a_2b_1)+b_2(a_1a_3+a_2)\\ \gamma_{den}&=b_1(a_1b_2+a_2b_1)-b_2(a_1a_3+a_2)\end{aligned} \tag{43}$$

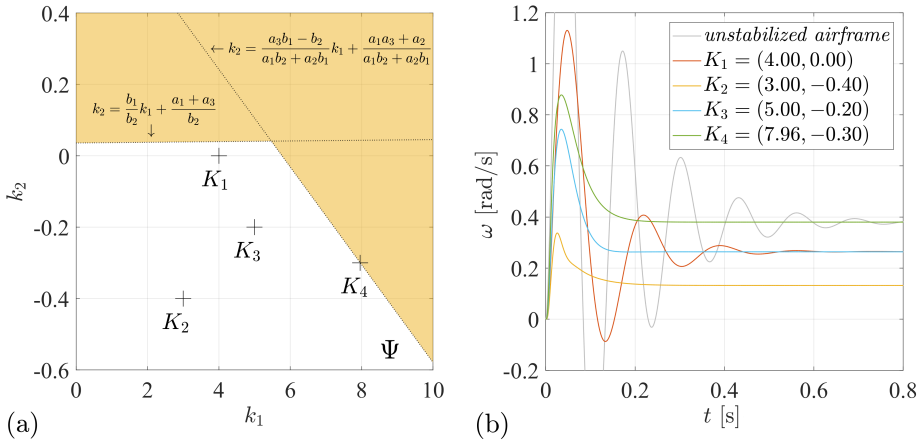

Fig. 2 (a) Area Ψ under consideration and examples of point pairs (k_1, k_2); and (b) system's step responses for the commanded fin deflections

calculated for the set of coefficients (5) with constant ("frozen") values, describing the state of the considered system in a finite, short time horizon, and following along lines (41) and (42), a (k_1, k_2) pair is sought for which

$$J_\Omega = \min\left\{\int_0^{t_f} (\omega - \omega_{st})^2 \, \mathrm{d}t\right\} \tag{44}$$

where ω is the angular rate of the airframe in current time t, ω_{st} is the angular rate of the airframe in a steady state for the constant values of the set of coefficients (5), and t_f is the simulation time. Since the coefficients (5) are functions of time in general, the pair (k_1, k_2) can be found in pre-processing mode, then tabulated or described by polynomial functions and used by the algorithm when the terminal phase of guidance is activated. This is advantageous from the point of view of hardware and software implementation and reduces requirements related to the computing power of the on-board processing unit.

2.4 System Stability

The classic Hurwitz criterion is used to consider the stability of the system. By multiplying the expressions in brackets of Eq. (35), we obtain the following:

$$s^4 + (\zeta_1 + 2\varsigma)s^3 + (2\varsigma\zeta_1 + \zeta_0 + \varsigma^2)s^2 + (\varsigma^2\zeta_1 + 2\varsigma\zeta_0)s + \varsigma^2\zeta_0 = 0 \tag{45}$$

Meeting conditions (39) and (40) means that $\zeta_1 > 0$ and $\zeta_0 > 0$, which means that all coefficients of Eq. (45) are positive. The determinants created from the coefficients of Eq. (45) have the following form:

$$\Delta_1 = |\zeta_1 + 2\varsigma| = \zeta_1 + 2\varsigma \tag{46}$$

$$\Delta_2 = \begin{vmatrix} \zeta_1 + 2\varsigma & 1 \\ \varsigma^2\zeta_1 + 2\varsigma\zeta_0 & 2\varsigma\zeta_1 + \zeta_0 + \varsigma^2 \end{vmatrix} = 2\varsigma^3 + 4\varsigma^2\zeta_1 + 2\varsigma\zeta_1^2 + \zeta_1\zeta_0 \tag{47}$$

$$\Delta_3 = \begin{vmatrix} \zeta_1 + 2\varsigma & 1 & 0 \\ \varsigma^2\zeta_1 + 2\varsigma\zeta_0 & 2\varsigma\zeta_1 + \zeta_0 + \varsigma^2 & \zeta_1 + 2\varsigma \\ 0 & \varsigma^2\zeta_0 & \varsigma^2\zeta_1 + 2\varsigma\zeta_0 \end{vmatrix} = \tag{48}$$
$$= 2\varsigma^5\zeta_1 + 4\varsigma^4\zeta_1^2 + 2\varsigma^3\left(\zeta_1^3 + 2\zeta_1\zeta_0\right) + 4\varsigma^2\zeta_1^2\zeta_0 + 2\varsigma\zeta_1\zeta_0^2$$

$$\Delta_4 = \begin{vmatrix} \zeta_1 + 2\varsigma & 1 & 0 & 0 \\ \varsigma^2\zeta_1 + 2\varsigma\zeta_0 & 2\varsigma\zeta_1 + \zeta_0 + \varsigma^2 & \zeta_1 + 2\varsigma & 1 \\ 0 & \varsigma^2\zeta_0 & \varsigma^2\zeta_1 + 2\varsigma\zeta_0 & 2\varsigma\zeta_1 + \zeta_0 + \varsigma^2 \\ 0 & 0 & 0 & \varsigma^2\zeta_0 \end{vmatrix} = \tag{49}$$
$$= \varsigma^2\zeta_0\left(\zeta_1 + 2\varsigma\right)\left(\varsigma^2\zeta_1 + 2\varsigma\zeta_0\right)\left(2\varsigma\zeta_1 + \zeta_0 + \varsigma^2\right)$$

As $\zeta_1 > 0$, $\zeta_0 > 0$ and $\varsigma > 0$, this entails $\Delta_i > 0$, $i \in \{1,2,3,4\}$, which means that the system is stable.

2.5 Compensation of System Gain Variability

During its flight, characteristics of the airframe undergo significant changes. In particular, the systematic decrease in the missile velocity when travelling through dense layers of the atmosphere causes significant differences in the values of coefficients described by Eq. (5). Therefore, it is necessary to include in Eq. (34) additional reinforcements compensating for this phenomenon and maintaining the achieved angular rate of the airframe at the set level:

$$\boldsymbol{K} = \begin{bmatrix} k_1 + \Delta k_1 & k_2 + \Delta k_2 \end{bmatrix} \tag{50}$$

Given the above, maintaining constant values of ζ_1 and ζ_0 throughout the entire guidance process is posited, in accordance with the following equations:

$$\zeta_1 = \acute{a}_1 + \acute{a}_3 + \acute{b}_1 k_1 - \acute{b}_2 k_2 = a_1 + a_3 + b_1\left(k_1 + \Delta k_1\right) - b_2\left(k_2 + \Delta k_2\right) \tag{51}$$

$$\begin{aligned} \zeta_0 &= \acute{a}_1\acute{a}_3 + \acute{a}_2 + \left(\acute{a}_3\acute{b}_1 - \acute{b}_2\right)k_1 - \left(\acute{a}_1\acute{b}_2 + \acute{a}_2\acute{b}_1\right)k_2 = \\ &= a_1a_3 + a_2 + \left(a_3b_1 - b_2\right)\left(k_1 + \Delta k_1\right) - \left(a_1b_2 + a_2b_1\right)\left(k_2 + \Delta k_2\right) \end{aligned} \tag{52}$$

where the symbol $\acute{(\cdot)}$ denotes the values of individual coefficients for $t = 0$, which is the beginning of the terminal phase of guidance of the missile against an aerial target.

After transforming (51) and (52), expressions for correction coefficients Δk_1 and Δk_2 in Eq. (50) ultimately take the following forms:

$$\Delta k_1 = \frac{\left(a_1b_2 + b_2\right)\mathrm{A} + b_2\mathrm{B} + a_2b_1}{b_1b_2\left(a_3 - a_1\right) - b_2^2 - a_2b_1^2} \tag{53}$$

$$\Delta k_2 = \frac{\Delta k_1 b_1 + \mathrm{A}}{b_2} \tag{54}$$

where

$$\mathrm{A} = a_1 - \acute{a}_1 + a_3 - \acute{a}_3 + \left(b_1 - \acute{b}_1\right)k_1 - \left(b_2 - \acute{b}_2\right)k_2 \tag{55}$$

$$\begin{aligned} \mathrm{B} = a_1a_3 - \acute{a}_1\acute{a}_3 + a_2 - \acute{a}_2 + \left(a_3b_1 - \acute{a}_3\acute{b}_1 - b_2 + \acute{b}_2\right)k_1 + \\ - \left(a_1b_2 - \acute{a}_1\acute{b}_2 + a_2b_1 - \acute{a}_2\acute{b}_1\right)k_2 \end{aligned} \tag{56}$$

Fig. 3a illustrates the values of corrections Δk_1 and Δk_2 as a function of time for the following exemplary coefficient initial values: $a_1 = 5\ \mathrm{s}^{-1}$, $a_2 = 2\,350\ \mathrm{s}^{-2}$, $a_3 = 10\ \mathrm{s}^{-1}$, $b_1 = 0.4\ \mathrm{s}^{-1}$, $b_2 = 420\ \mathrm{s}^{-2}$. Figs 3b-3d show system step responses to the commanded canard fin deflections for successive sets of coefficients given by Eqs (5) and treated as constants in the short time horizon for: unstabilized airframe (U), airframe equipped with a state observer based stabilization system (SO), and airframe equipped with SO system and associated correction part (SO+CP). Both systems correctly perform the stabilization task (Figs 3c-3d in relation to Fig. 3b). However, it should be noted that, unlike the SO system, the SO+CP system strives to maintain a constant angular rate of the airframe for a given value of the input signal, regardless of changes in the characteristics of the missile and environmental parameters (cf. Figs 3c-3d).

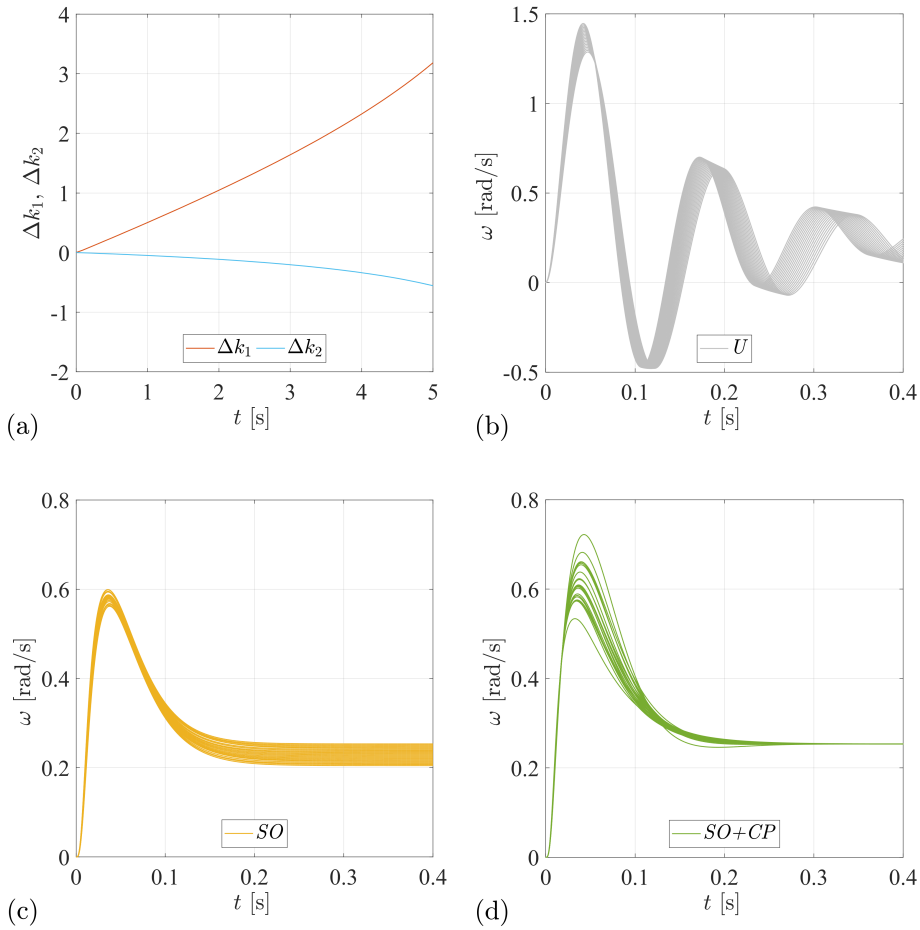

Fig. 3 (a) Example values of correction coefficients Δk_1 and Δk_2. System responses to the step deflection of canard fins for: (b) unstabilized airframe; (c) airframe with an SO system; and (d) airframe with an SO+CP system

3 Results and Discussion

In Section 3, a comparison of the performance of the stabilization systems just developed is made for: a) missile airframe stabilized by proposed state observer (SO) with initial values k_1 = 8.11 and $k_2 = -0.32$; and b) missile airframe stabilized by proposed state observer with initial values k_1 = 8.11 and $k_2 = -0.32$ and correction part (SO+CP) given in Subsection 2.5. To provide a reference, the scenarios are examined against a missile airframe stabilized by a classical Raytheon three-loop autopilot (TLA) with parameter values K_O = 830, K_A = 0.012, K_I = 0.035 and K_P = 0.1. Symbols for TLA are taken in accordance with [8]. Note that detailed discussion about TLA structure and parameter selections can be found in the respective literature, cf. e.g. [6, 7, 9, 10]. Moreover, for some general tests, the results achieved for an unstabilized missile airframe (U) are also included to provide a physical background of the considered problem.

The proposed stabilization system solutions are examined for the terminal guidance phase. First, a basic examination of the proposed structures is performed using the sample run test. Next, a missile-target engagement scenario and Monte Carlo simulation study are carried out to evaluate and compare the performance of the solutions. The fourth-order Runge-Kutta numerical integration method is used for the derivation of approximating differential equations for the elements of the system.

3.1 Sample Run Test

Firstly, the results obtained as step responses of the missile airframes equipped with SO, SO+CP and TLA stabilization systems will be discussed. The initial missile velocity is assumed to be V = 950 m/s and changes in time as follows:

$$\dot{V} = -\frac{\rho V^2}{2m} S \left[c_0 + \mu \left(c_L^{\alpha} \alpha \right)^2 \right] \tag{57}$$

where c_0 is the zero-lift drag coefficient [–], and μ is the induced drag coefficient [-–]. The canard deflection angle is bounded to $|\delta| < 0.35$ rad and the canard servo is characterized by a time constant of τ = 0.01 s. The missile model parameters for t = 0 are: a_1 = 5 s^{-1}, $a_2 = 2350 s^{-2}$, a_3 = 10 s^{-1}, $b_1 = 0.4$ s^{-1}, b_2 = 420 s^{-2}, and are time-variable as presented in Fig. 4a.

The results presented in Fig. 4b highlight the essence of the operation of the designed stabilization systems whose fundamental task is to make the value of the output signal independent of the dynamic characteristics of the airframe. In the case of the unstabilized airframe, the changes in the values of the parameters describing the airframe dynamics cause the angular rate ω to decrease over time, in spite of the fact that the control signal κ at the input to the system remains constant.

In the case of the missile equipped with the SO stabilization system, an unfavorable phenomenon is evident in the form of a reduction of the achieved value of angular rate ω of the airframe during the flight, similarly as in the case of an unstabilized airframe (disregarding oscillations). On the other hand, the SO+CP and TLA systems consistently maintain the achieved value of the angular rate ω at a constant level. Both of the proposed stabilization systems (SO and SO+CP) are characterized by better dynamic responses than the solution based on the classic TLA.

Figs 5-6 show the graphs of angular rate ω, angle of attack α, and canard deflection angle δ obtained as a result of the response of missile airframes with SO, SO+CP and TLA

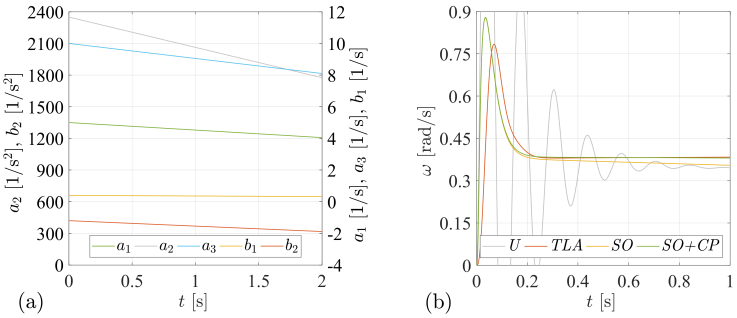

Fig. 4 (a) Changes in the coefficients of Eq. (5); and (b) step responses of the considered systems

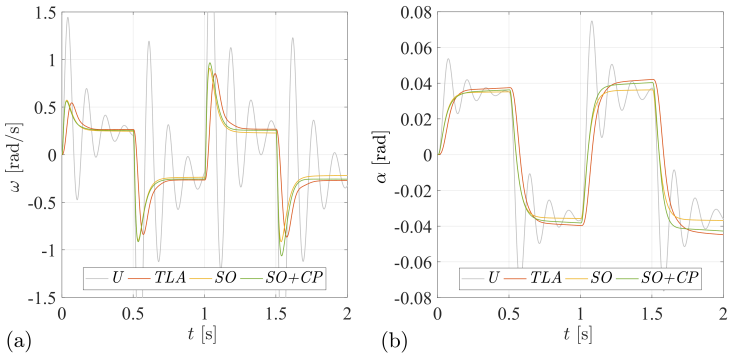

Fig. 5 (a) Airframe angular rate; and (b) angle of attack histories for a sample run test

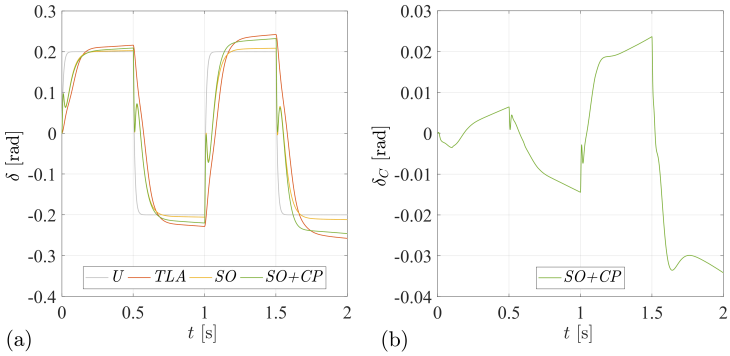

Fig. 6 (a) Canard-fin deflection angle histories for a sample run test; and (b) canard-fin deflection angle correction for SO+CP system

systems to an applied test signal. A symmetric rectangular signal with values ±0.2 rad and a 50% duty cycle was input to the system, simulating stepped, alternating canard-fin deflections.

The following conclusions can be drawn from the results obtained. Fig. 5 shows that, generally speaking, each of the systems under consideration is capable of stabilizing the missile airframe, resulting among others in the smooth course of transitional processes (Fig. 5a), and has a beneficial effect on changes to the angle of attack (Fig. 5b). Similarly to Fig. 4b, the airframe angular rate reduction effect in the SO system is also clearly visible here (Fig. 5a). With regard to the TLA and SO+CP systems, the angular rate of the airframe workes without error, and the SO+CP system reaches the set value by about 0.08 s faster. Efforts made by both systems to maintain the desired value of the angular rate of the airframe result in a gradual increase of the canard fin deflections (Fig. 6a). This also occurs in the case of the SO system, but here the process is much slower, resulting in a gradual decrease in the angular rate over time. On the other hand, lower maximum values of canard fin deflections are observed in the SO+CP system than in the TLA system, while maintaining greater efficiency of angular rate obtainment. The physical barrier is $|\delta_{\max}|$, beyond which the impact of the systems under consideration on the missile airframe becomes limited. The signal introduced by the correction part of the SO+CP system is about 10% of the total value of the control signal (Fig. 6b).

3.2 Missile-Target Engagement Scenario

It is assumed that the missiles are aimed at the target performing a sinus-wave evasive maneuver. The initial range between target and missiles was chosen as 4 800 m. At the time t = 0 (i.e. beginning of guidance terminal phase), the target is located at the pitch angle $\theta_T = \pi/7$ rad, at the course angle $\phi_T = 3\pi/4$ rad and is moving with initial velocity V_T = 220 m/s at a height of 4 000 m. The dynamics of the target is characterized by the time constant τ_T = 1 s for each of the control planes. During the flight, the target velocity and acceleration profiles are changing as presented in Fig. 7, in which V_T is the target velocity, and n_L, n_θ, n_ϕ are longitudinal, pitch plane and yaw plane accelerations, respectively. The scenario was constructed in such a way as to ensure that each missile is able to reach the rendezvous point with an acceptable value of the miss distance. It is assumed that the missiles have no thrust during the endgame. The missile airframe coefficients, initial velocity, and canard fins parameters are taken as in Subsection 3.1.

Data supply for the coordinate determination system is provided by the missile seeker. The signal returned by the seeker contains information about the angular rate of the line of sight (LOS) distorted by the inertia of the seeker system, by the signal proportional to the angular acceleration of the missile airframe, and by generally understood measurement errors, and is taken for a control plane as [3]

$$\dot{\lambda}_m = \frac{k_s}{\tau_s}(\lambda + \Delta\lambda + \chi\omega - \lambda_m) \tag{58}$$

where λ and λ_m are the actual and measured LOS angles; χ = 0.1 ms is the sampling period; k_s = 1 and τ_s = 5 ms are the gain and the time constant of the seeker drives; and $\Delta\lambda$ denotes the sum of fluctuating interferences caused by the noise from on-board devices, mechanical vibrations, and the environment.

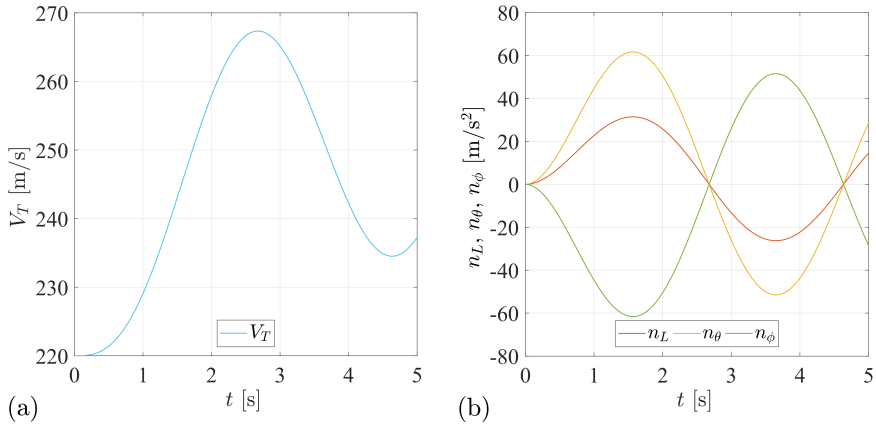

Fig. 7 Aerial target: (a) velocity; and (b) acceleration profiles

The simulations were conducted in the absence and in the presence of these disturbances taken as band-limited white-noise with power spectral density (PSD) between -50 and -30 dBm/Hz. The classical proportional navigation (PN) control law is applied to guide the missiles to the aerial target:

$$\kappa = \eta V_C \dot{\lambda} \tag{59}$$

where κ is the command in the control plane, η is the gain coefficient dependent on mass-geometrical characteristics of the missile airframe and including a navigation constant $n = 3$, and V_C is the closing velocity. No predicted intercept point (PIP) is calculated.

The missiles have been evaluated against the miss distance d, target interception time t_f, and quantity indices w, A, and Q. The miss distance d is defined as

$$d = \sqrt{(x_T - x_M)^2 + (y_T - y_M)^2 + (z_T - z_M)^2} \tag{60}$$

where x_T, y_T and z_T are the coordinates of the instantaneous position of the target, and x_M, y_M and z_M are the coordinates of the instantaneous position of the missile at the time instant at which the closing velocity V_C changed the sign. The quality indices w, A and Q are chosen to be

$$w = \sqrt{a_\theta^2 t_f + a_\phi^2 t_f} \tag{61}$$

$$A = \int_0^{t_f} \boldsymbol{a}^{\mathrm{T}} \boldsymbol{a} \, \mathrm{d}t \qquad \text{and} \qquad \boldsymbol{a} = \begin{bmatrix} a_\theta & a_\phi \end{bmatrix} \tag{62}$$

$$Q = \int_0^{t_f} \boldsymbol{q}^{\mathrm{T}} \boldsymbol{q} \, \mathrm{d}t \qquad \text{and} \qquad \boldsymbol{q} = \begin{bmatrix} \omega_\theta - \dot{\theta} & \omega_\phi - \dot{\phi} \end{bmatrix} \tag{63}$$

where $\boldsymbol{a}$ is a two-element vector of missile airframe accelerations in control planes and $\boldsymbol{q}$ is a two-element vector containing differences between airframe angular rate and velocity vector angular rate in pitch and yaw plane, respectively. The symbols in Eqs (61)-(63) have the following meanings: t_f is the target interception time; a_θ and a_ϕ are missile airframe

accelerations in pitch and yaw plane; θ and ϕ are the pitch and yaw angle of the missile velocity vector; ω_θ and ω_ϕ are the angular rates of the missile airframe in pitch and yaw plane, respectively.

The engagement geometry and trajectories are plotted in Fig. 8 using a specialized Matlab package described in [30]. Simulation results for the case of no disturbances are presented in Tab. 1 and Figs 9-12. In Figs 10-12, the vertical dashed line marks the average time of target interception.

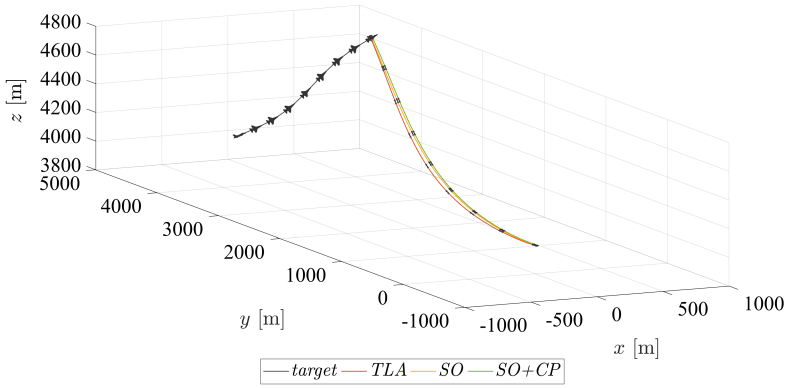

Fig. 8 Missile and target trajectories

Tab. 1 Results for the missile-target engagement scenario

Missile model	t_f **[s]**	d **[m]**	w **[m/s^2]**	A **[m^2/s^3]**	Q **[rad^2/s]**
SO+CP	4.7860	3.40	43.37	3.69×10^8	440.77
SO	4.7862	3.40	42.59	3.65×10^8	441.12
TLA	4.7910	3.37	30.48	3.88×10^8	153.35

The simulation conditions were deliberately selected so as to ensure that the results of the guidance process obtained in the first attempt are as similar to each other as possible, i.e. to obtain a consistent starting point for further simulations using the TLA, SO and SO+CP systems. For this purpose, a relatively undemanding aerial target was selected, moving at a low velocity and with medium accelerations. The mutual initial position of the missiles and the target was also set in such a way so that all three missiles could successfully intercept the target with the smallest possible miss distance (Fig. 8). The simulation shows that the angular rates of the airframes equipped with SO and SO+CP systems changed within slightly smaller limits than the missiles with the TLA system (Fig. 9), which should have a positive effect on the operating conditions of the seeker and the effectiveness of the whole guidance process in the next scenarios. It is worth noting that during most of the guidance process, missiles equipped with the SO and SO+CP systems moved with lower values of the angles of attack and sideslip, normal accelerations and canard fin deflections than the missile with the TLA system, which is a positive effect in

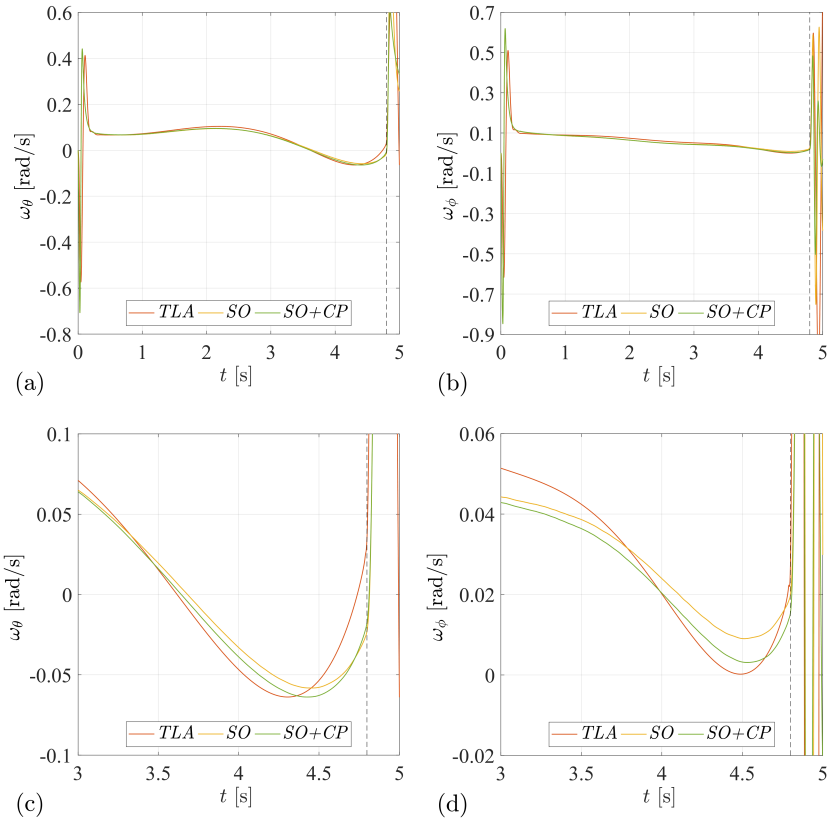

Fig. 9 Missile airframe angular rates in: (a) pitch plane; and (b) yaw plane. Details for: (c) pitch plane; and (d) yaw plane

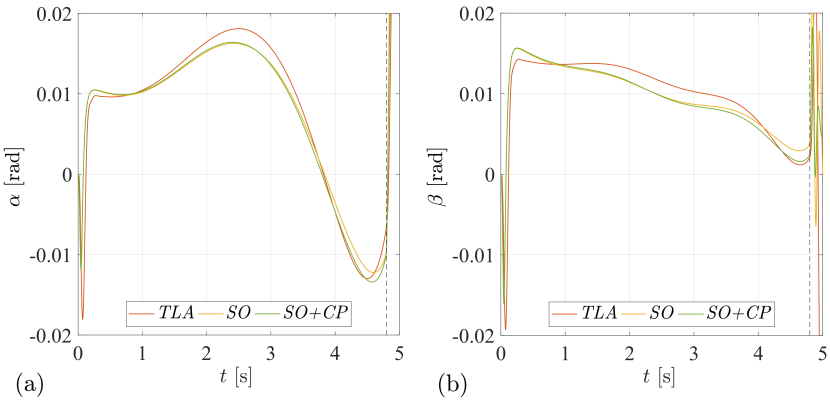

Fig. 10 Missile airframe: (a) angle of attack; and (b) sideslip

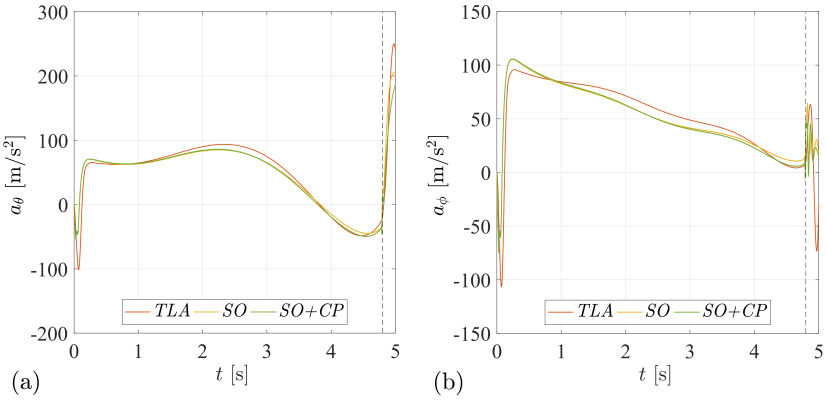

Fig. 11 Normal accelerations of missile airframe in: (a) pitch plane; and (b) yaw plane

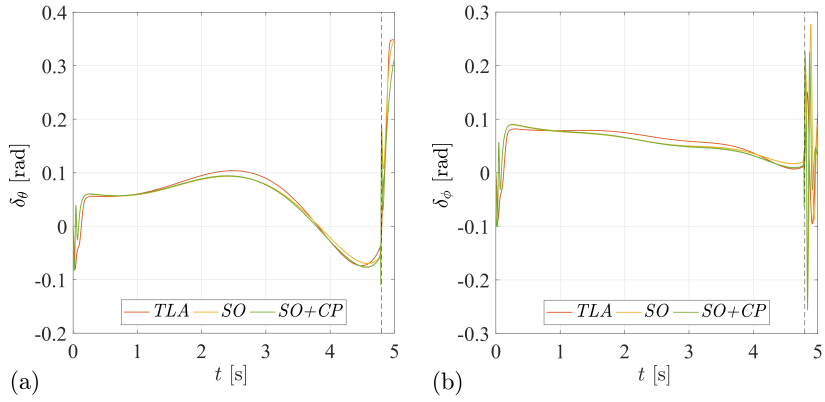

Fig. 12 Canard deflection angles in: (a) pitch plane; and (b) yaw plane

terms of energy considerations (Figs 10-12). As originally assumed, comparable simulation results were achieved: target interception time $t_f \approx 4.79$ s for all cases, miss distance $d \approx 3.4$ m (cf. Table 1). In some respects, the missile equipped with the TLA system achieved slightly better results (ca. 12 m/s^2 lower normal acceleration w at the moment of target interception, a more favorable value of the quality index Q). In turn, the values of the quality index A definitely speak in favor of the SO and SO+CP systems, which is a direct consequence of the acceleration histories shown in Fig. 11.

To demonstrate the advantages of the proposed stabilization system, the scenario presented above was considered for the presence of disturbances in the signal processing path, with a PSD value selected from a range of -50 to -30 dBm/Hz. Selected simulation results are presented in Tab. 2 and Figs 13-14. These results enable the formulation of the conclusions below.

The greatest effort of the stabilization systems is observed in the presence of disturbances with a PSD of approximately -35 dBm/Hz -the threshold value for the success of the homing process, understood as obtaining a miss distance $d \leq 5$ m (an arbitrary value adopted for the purposes of considerations, equal to the assumed effective range of the missile's warhead). In particular, Fig. 13b shows a breakdown of the characteristics, which proves that above the limit of -35 dBm/Hz, the analyzed systems are unable to compensate for miss distance d, which in each of the considered cases assumes unacceptable values from a military point of view. The proposed SO and SO+CP systems show a two- to three-times improved efficiency in terms of compensating for the miss distance in the presence of interference than the classic TLA system, while significantly reducing the values of the required control accelerations (cf. Fig. 13 and Tab. 2), which is reflected in the values of the obtained quantity index A (Fig. 14a). At the same time, in the case of the SO and SO+CP systems, higher values of the index Q were noted than in the case of TLA, which is associated with greater temporary differences between the angular rate of the airframe and the angular rate of the velocity vector at the beginning of the guidance process (Figs 9a-9b and Fig. 14b).

Tab. 2 Results for the missile-target engagement scenario (cont.)

Missile model	**PSD [dBm/Hz]**	t_f **[s]**	d **[m]**	w **[m/s^2]**	A **[m^2/s^3]**	Q **[rad^2/s]**
SO+CP		4.7857	3.40	36.01	3.51×10^8	180.25
SO	-50	4.7858	3.40	31.62	3.47×10^8	180.39
TLA		4.7906	3.37	33.92	3.76×10^8	78.34
SO+CP		4.7908	3.36	69.74	3.71×10^8	185.68
SO	-40	4.7912	3.36	81.08	3.77×10^8	195.42
TLA		4.7981	3.34	144.37	4.92×10^8	140.75
SO+CP		4.8005	5.26	184.44	5.88×10^8	415.39
SO	-35	4.8019	6.80	193.94	6.27×10^8	429.45
TLA		4.8145	18.86	293.11	8.85×10^8	364.56
SO+CP		4.8177	56.28	195.11	8.35×10^8	1363.37
SO	-30	4.8186	66.73	158.64	8.36×10^8	1523.41
TLA		4.8362	118.02	250.68	1.00×10^9	1067.52

3.3 Monte Carlo Simulation Study

To evaluate and compare the performance of the proposed solutions, a Monte Carlo simulation study consisting of 500 sample runs for each stabilization system was carried out. In these simulations, initial target and missile positions, orientations and parameters are taken as described in Subsection 3.2. The aerial target control commands perform a square-wave evasive maneuver with a period of ΔT and a phase of $\Delta\varphi$ relative to the $t = 0$. For each test case, the random variables were chosen to be the target time constant τ_T, its initial velocity V_T, pitch angle θ_T and course angle ϕ_T (Tab. 3 and Fig. 15). These variables were assumed to be distributed uniformly.

The missiles for each sample run have been evaluated against the quantity indices defined by Eqs (60)-(63). The collective simulation results are given in Tab. 4, in which:

DOI 10.3849/aimt.01858

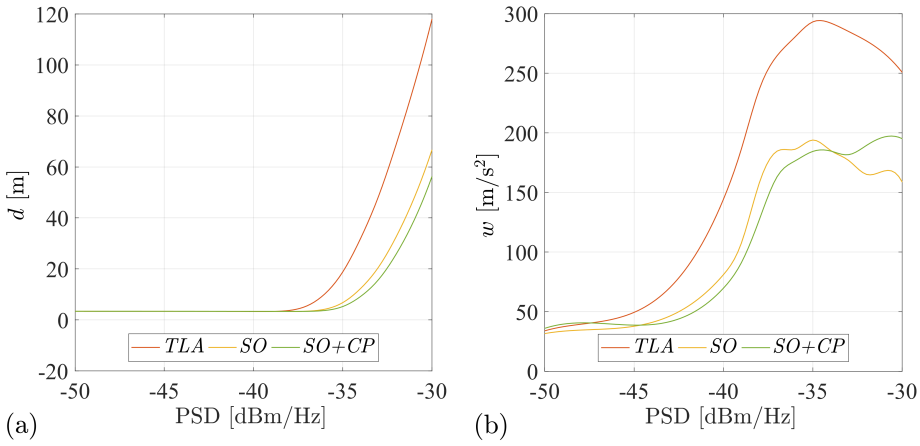

Fig. 13 (a) Miss distances; and (b) airframe normal accelerations for different values of disturbances

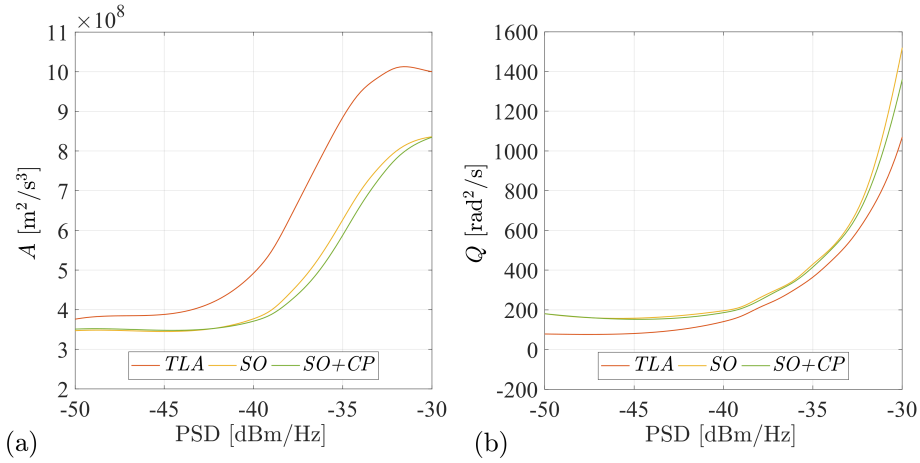

Fig. 14 Quantity indices: (a) A; and (b) Q for different values of disturbances

$$\bar{t}_f = \frac{1}{500}\sum_{i=1}^{500} t_{fi} \qquad \bar{d} = \frac{1}{500}\sum_{i=1}^{500} d_i \qquad \bar{w} = \frac{1}{500}\sum_{i=1}^{500} w_i$$
$$\bar{A} = \frac{1}{500}\sum_{i=1}^{500} A_i \qquad \bar{Q} = \frac{1}{500}\sum_{i=1}^{500} Q_i \tag{64}$$

describe the mean values of target interception time t_f and quantity indices defined by Eqs (60)-(63), respectively, for each of considered missiles. In Figs 16-17 the miss distances are plotted for different dynamic capabilities of the aerial target.

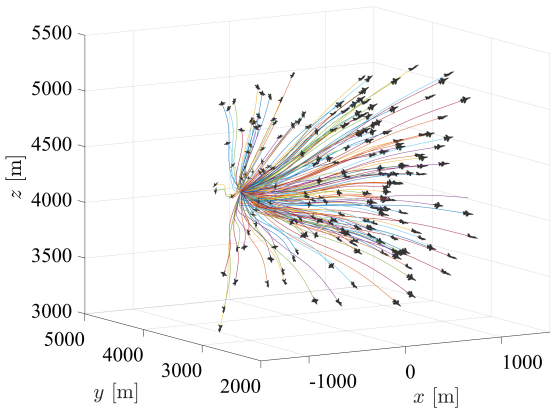

Fig. 15 Set of aerial target trajectories for Monte-Carlo simulation study (only 200 of 500 generated are shown for clarity)

Tab. 3 Target initial parameter ranges for Monte Carlo simulation study

Parameter	Symbol	Unit	Min	Max
time constant	τ_T	s	0.01	1.0
velocity	V_T	m/s	220	440
pitch angle	θ_T	rad	$-\pi/6$	$\pi/6$
course angle	ϕ_T	rad	$3\pi/4$	$5\pi/4$

Tab. 4 Results for Monte Carlo simulation study

Missile model	PSD [dBm/Hz]	$\bar{t}_f$ [s]	$\bar{d}$ [m]	$\bar{w}$ [m/s^2]	$\bar{A}$ [m^2/s^3]	$\bar{Q}$ [rad^2/s]
SO+CP		3.9605	4.17	126.49	3.89×10^8	363.95
SO	none	3.9606	4.16	121.65	3.86×10^8	382.96
TLA		3.9683	4.83	218.59	6.33×10^8	130.69
SO+CP		3.9605	4.16	121.69	3.79×10^8	194.22
SO	-50	3.9607	4.16	111.09	3.75×10^8	197.03
TLA		3.9681	5.88	220.03	6.23×10^8	84.46
SO+CP		3.9634	4.12	140.75	4.11×10^8	190.28
SO	-40	3.9636	4.12	126.75	4.13×10^8	191.70
TLA		3.9721	28.39	278.57	7.80×10^8	148.06
SO+CP		3.9680	7.26	244.67	6.44×10^8	378.40
SO	-35	3.9684	8.20	254.34	6.67×10^8	391.43
TLA		3.9755	86.74	272.83	8.42×10^8	341.38

Fig. 16 shows the miss distance as a function of the target velocity at the intercept point. All considered stabilization systems are characterized by a similar performance in the absence of disturbances and with a relatively low velocity of the target under attack (miss distance value below 5 m for a target moving at a velocity of 220 m/s), which

DOI 10.3849/aimt.01858

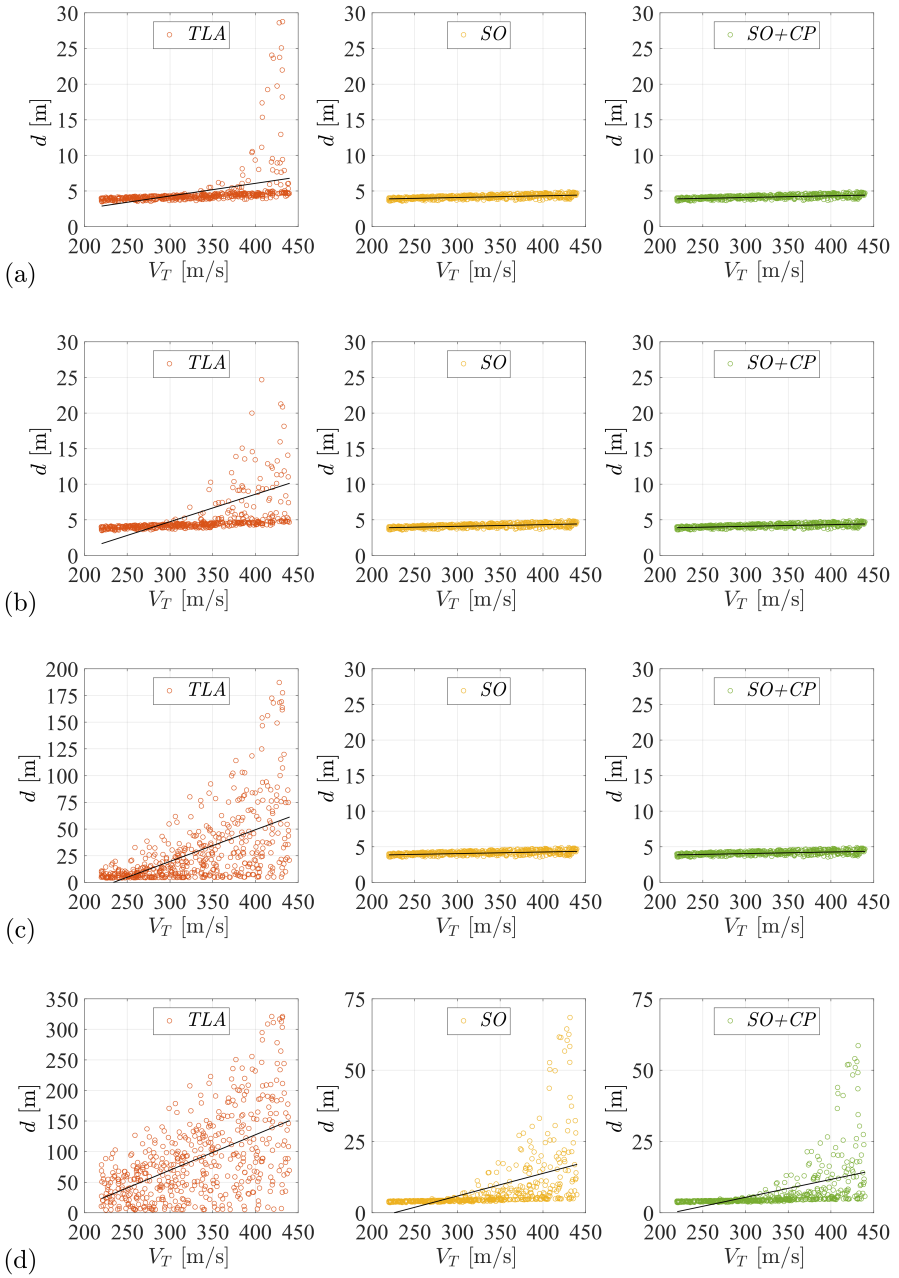

Fig. 16 Miss distance distributions and trend lines for different target velocity: (a) without disturbances; and in the presence of noise with PSD equal to: (b) −50 dBm/Hz; (c) −40 dBm/Hz; and (d) −35 dBm/Hz

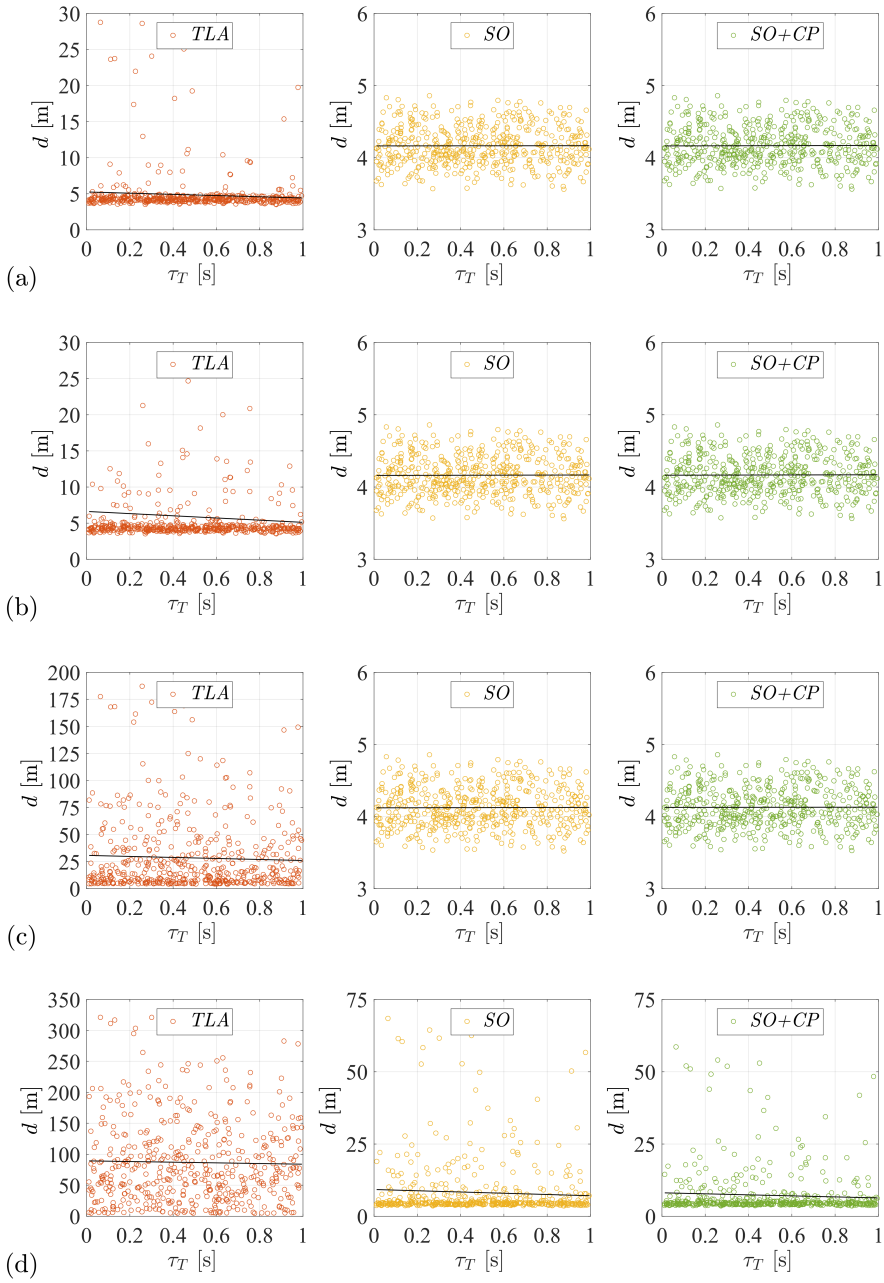

Fig. 17 Miss distance distributions and trend lines for different target dynamics: (a) without disturbances; and in the presence of noise with PSD equal to: (b) −50 dBm/Hz; (c) −40 dBm/Hz; and (d) −35 dBm/Hz

gives a common starting point for the discussion on the assessment of their capabilities (Fig. 16a). Please note that as the velocity of the target increases, the effectiveness of the TLA system decreases, which directly translates into the final miss distance value. In the extreme case, it reaches a value of almost 30 m (for a target moving at a velocity of 440 m/s). In contrast to the TLA, the SO and SO+CP systems maintain their effectiveness when guiding targets moving at high velocities, and the average miss distance for the entire aerial target velocity range under consideration is below 5 m. The differences between the analyzed stabilization systems deepen with the increase of disturbances in the measurement path (Figs 16b-16d). It is worth emphasizing that the proposed SO and SO+CP systems correctly perform the stabilization task in the event of an increase in the disturbance signal, and for the value of -35 dBm/Hz it is possible to effectively guide missiles against an aerial target moving at a velocity of up to 300 m/s (Fig. 16d). This capability is lost in the case of the TLA system at disturbances with a PSD of -50 dBm/Hz (Fig. 16b).

In turn, Fig. 17 shows the miss distance as a function of the target's maneuverability characterized by the time constant τ_T. The SO and SO+CP systems maintain the ability to stabilize the airframe characteristics in the entire range of considered changes in the aerial target dynamics, both in the absence (Fig. 17a) and in the presence of disturbances in the measurement path (Figs 17b-17d). The miss distance under disturbances of -40 dBm/Hz in no case exceeded the value of 5 m. In turn, for the TLA system, an average miss distance of 28.39 m was achieved under these conditions, with a maximum value of 185.25 m, which is absolutely unacceptable from a military point of view.

The unfavorable effect of noise at the PSD equal to -35 dBm/Hz is already clearly visible in the case of all three considered stabilization systems (Fig. 17d). However, it should be emphasized that in the case of the SO and SO+CP systems, in the majority (about 80%) of the performed scenarios, the final miss distance of less than 5 m was obtained, with an average of 7.26 m for the SO+CP system and 8.20 m for the SO system. Under these conditions, the TLA system basically loses its ability to affect the missile airframe.

Simulation results also showed, in the case of SO and SO+CP systems, more favorable average values of acceleration $\bar{w}$ at the missile-target meeting point and index $\bar{A}$ with an indication of the advantage of the SO+CP solution over SO when disturbance level increases (Tab. 4). The averaged index $\bar{Q}$ is in favor of the TLA system and confirms the conclusions presented in Subsection 3.2.

The fact that no run presented in Figs 16-17 achieves zero miss distance value and the mean values are about 4 m in best cases requires some explanation. First of all, airframe stabilization systems are just a part of the autopilot and are not able to reduce the miss distance to zero independently. Their main task is to protect the on-board seeker before the influence of dynamic changes, which exert a negative interaction on the homing process. Next, in case under consideration, the simplest version of the proportional navigation (PN) guidance method is used and no predicted intercept points (PIP) are calculated. This approach is intended to limit considerations to issues related to the stabilization systems, and leave aside the discussion of a number of complex problems related to the optimal design of the guidance loop. Last but not least, there are inertial components in the assumed guidance loop, e.g., from the seeker drives and actuators, so there are always differences between measured and real target positions because of a signal processing lag, which are

especially evident in the case of maneuvering targets. Please note that an extended discussion of this problem is presented in one of author's previous studies [3].

4 Conclusions

This paper describes the use of a state observer with a correction part to stabilize the static and dynamic characteristics of the airframe of a canard-controlled anti-aircraft missile. An analytical method of determining the entries of the feedback-loop gain matrix $\boldsymbol{K}$ is outlined, both for state observer based (SO) and state observer with correction part (SO+CP) system solutions.

The proposed stabilization system provides a wide range of possibilities for supporting missile guidance process in changing conditions of an aerial combat situation, including high dynamics of the aerial target and disturbances in signal processing paths. Its advantages include, among others, a reduction in energy losses resulting from a decrease of the angle of attack values during the whole guidance process. Moreover, the airframe transitional processes become shorter and smoother, leading to better operating conditions for the seeker installed on board the missile and an overall improved performance result of the guidance process towards an aerial target. On one hand, this allows the missile to maintain the required miss distance value and leads to a slight reduction in the homing time. On the other, missile airframe normal accelerations at the intercept point achieved by SO and SO+CP systems are two times, on average, smaller than those produced by TLA. This creates a kind of maneuvering reserve of the missile, which can be used when homing on high-maneuvering targets.

The efficiency of the SO+CP stabilization system in relation to the SO grows with the increase of disturbance level in the signal path (in the considered range). However, it should be emphasized that even in the case of significant differences between the current parameters of the airframe and the parameters of its model in the state observer loop (which could be observed in the case of the presented SO system), the stabilization loop develops the correct settings of the canards, ensuring the required angular position of the missile in space.

The proposed algorithm is relatively easy to implement and is undemanding of significant processor resources. Technical implementation gives rise obviously several practical and hardware problems. Discussion of these issues is, however, beyond the scope of this paper.

Future work will be aimed at searching for a solution combining the developed stabilization system with modern guidance methods to lead to a direct hit of the aerial target and to destroying it using a hit-to-kill mechanism.

Funding

This work was financed by Military University of Technology under research project UGB 22-825/2023.

References

[1] GRYCEWICZ, H., R. MOSIEWICZ and J. PIETRASIEŃSKI. *Radio Control Systems*. Warsaw: Military University of Technology, 1984.

[2] HONG, J.H., S.S PARK, C.H. LEE and C.K. RYOO. Study on Parasite Effect with Strapdown Seeker in Consideration of Time Delay. *Journal of Guidance, Control, and Dynamics*, 2019, **42**(6), pp. 1383-1392. DOI 10.2514/1.G004040.

[3] BUŻANTOWICZ, W. Tuning of a Linear-Quadratic Stabilization System for an Anti-Aircraft Missile. *Aerospace*, 2021, **8**(2), p. 48. DOI 10.3390/aerospace8020048.

[4] KOPP, C. Genesis of the Surface-to-Air Missile. *Defence Today*, 2006, **5**(5), pp. 9-11.

[5] ZARCHAN, P. *Tactical and Strategic Missile Guidance*. 6th ed. Reston: AIAA, 2012. ISBN 978-1-60086-894-8.

[6] MRACEK, C.P. and D.B. RIDGLEY. Missile Longitudinal Autopilots: Comparison of Multiple Three Loop Topologies. In: *Proceedings of the AIAA Guidance, Navigation and Control Conference*. San Francisco: AIAA, 2005. DOI 10.2514/6.2005-6380.

[7] AGGARWAL, R. and D. BOUDREAU. An Implementable High-Order Guidance Law for Homing Missiles. In: *Proceedings of the* 34*th Conference on Decision and Control*. New Orleans: IEEE, 1995, pp. 1865-1866. DOI 10.1109/CDC.1995.480614.

[8] KIM, J.H. and I.H. WHANG. Augmented Three-Loop Autopilot Structure Based on Mixed-Sensitivity H_∞ Optimization. *Journal of Guidance, Control, and Dynamics*, 2018, **41**(3), pp. 748-753. DOI 10.2514/1.G003119.

[9] RUSNAK, I. and H. WEISS. New Control Architecture for High Performance Autopilot. In: *Proceedings of* 51*th Israel Annual Conference on Aerospace Sciences*. Tel Aviv and Haifa, 2011, pp. 679-696.

[10] ABD-ELATIF, M.A., L.J. QIAN and Y.M. BO. Optimization of Three-Loop Missile Autopilot Gain under Crossover Frequency Constraint. *Defence Technology*, 2016, **12**(1), pp. 32-38. DOI 10.1016/j.dt.2015.08.006.

[11] MARKIN, E. *Principles of Modern Radar Missile Seekers*. Norwood: Artech, 2022. ISBN 978-1-63081-777-0.

[12] PALUMBO, N.F., B.E. REARDON and R.A. BLAUWKAMP. Integrated Guidance and Control for Homing Missiles. *Johns Hopkins APL Technical Digest*, 2004, **25**(2), pp. 121-139.

[13] PALUMBO, N.F. Guest Editor's Introduction: Homing Missile Guidance and Control. *Johns Hopkins Apl Technical Digest*, 2010, **29**(1), pp. 2-8.

[14] BUŻANTOWICZ, W. and J. PIETRASIEŃSKI. Dual-Control Missile Guidance: A Simulation Study. *Journal of Theoretical and Applied Mechanics*, 2018, **56**(3), pp. 727-739. DOI 10.15632/jtam-pl.56.3.72.

[15] HU, S., J. WANG, Y. WANG and S. TIAN. Stability Limits for the Velocity Orientation Autopilot of Rolling Missiles. *IEEE Access*, 2021, **9**, pp. 110940-110951. DOI 10.1109/ACCESS.2021.3102083.

[16] KEDARISETTY, S. Novel Two Phase Algorithm to Design Three Loop Autopilot Using Parameter Plane Technique and Particle Swarm Optimization. *IFAC-PapersOnLine*, 2016, **49**(1), pp. 830-835. DOI 10.1016/j.ifacol.2016.03.161.

[17] SIOURIS, G.M. *Missile Guidance and Control Systems*. New York: Springer, 2010.ISBN 978-1-4419-1835-2.

[18] QIAN, H. and T. LI. Integrated Guidance and Control for Missiles with Three-Dimensional Impact Angle Constrained. *International Journal of Innovative Computing, Information and Control*, 2021, **17**(2), pp. 581-593. DOI 10.24507/ijicic.17.02.581.

[19] ZHANG, Q., L.Z. LIU, H. MA, Z. XU and X.Z. WANG. Design on Integrated Guidance and Control Considering the Constraint of Impact Angle and Input Saturation. *Journal of Ballistics*, 2021, **33**(3), pp. 9-18. DOI 10.12115/j.issn.1004-499X(2021)03-002.

[20] FU, Z., K. ZHANG and S. YANG. Research on Three-Dimensional Integrated Guidance and Control Design with Multiple Constraints. *International Journal of Aerospace Engineering*, 2022, 6296770. DOI 10.1155/2022/6296770.

[21] RADKE, A. and G. ZHIGIANG. A Survey of State and Disturbance Observers for Practitioners. In: *Proceedings of 2006 American Control Conference*. Minneapolis: IEEE, 2006 DOI 10.1109/ACC.2006.1657545.

[22] XIEYU, X., C. XIAOXI, Y. WENBO, L. PENGHAO and G. MI. Design of Missile Roll Autopilot based on Linear Extended State Observer. In: *Proceedings of the* 34^{th} *Chinese Control and Decision Conference (CCDC)*. Hefei: IEEE, 2022, pp. 418-421. DOI 10.1109/CCDC55256.2022.10033507.

[23] TIAN, J., S. ZHANG and H. YANG. Enhanced Extended State Observer based Control for Missile Acceleration Autopilot. *ISA Transactions*, 2020, **96**, pp. 143-154. DOI 10.1016/j.isatra.2019.06.009.

[24] HAN, D., C. LI and Z. SHI. Attitude Autopilot Design Based on Fuzzy Linear Active Disturbance Rejection Control. *Aerospace*, 2022, **9**(8), p. 429. DOI 10.3390/aerospace9080429.

[25] BHOWMICK, P. and G. DAS. Modification of Classical Two Loop Lateral Missile Autopilot Design Using Reduced Order Observer (DGO) and LQR. In: *Proceedings of* 3^{rd} *International Conference on Computing, Communication and Networking Technologies (ICCCNT 2012)*. Coimbatore: IEEE, 2012, pp. 1-6. DOI 10.1109/ICCCNT.2012.6395914.

[26] THEODOULIS, S. and G. DUC. Missile Autopilot Design Using Observer-based Gain Scheduling. *IFAC Proceedings Volumes*, 2007, **40**(7), 7pp. 98-803. DOI 10.3182/20070625-5-FR-2916.00136.

[27] AWAD, A. and H. WANG. Roll-Pitch-Yaw Autopilot Design for Nonlinear Time-Varying Missile Using Partial State Observer based Global Fast Terminal Sliding Mode Control. *Chinese Journal of Aeronautics*, 2016, **29**(5), pp. 1302-1312. DOI 10.1016/j.cja.2016.04.020.

[28] WANG, Y., W. WANG, H. LEI, J. LIU, B. CHEN and Y. ZHAO. Observer-based Robust Impact Angle Control Three-Dimensional Guidance Laws with Autopilot Lag. *Aerospace Science and Technology*, 2023, 108505. DOI 10.1016/j.ast.2023.108505.

[29] LEE, H., X. HUANG and H. YIN. Enhanced Sliding Mode Control for Missile Autopilot Based on Nonlinear Disturbance Observer. In: *Proceedings of 2009 International Joint Conference on Computational Sciences and Optimization*. Sanya: IEEE, 2009, pp. 210-213. DOI 10.1109/CSO.2009.29.

[30] BUŻANTOWICZ, W. Matlab Script for 3D Visualization of Missile and Air Target Trajectories. *International Journal of Computer and Information Technology*, 2016, **5**(5), pp. 419-422. ISSN 2279-0764.